machines

MDPI

Article

CO_2 Footprint Reduction in Hydraulically Driven Industrial Machinery: Applications of a Sustainability-Conscious Management Strategy Based on a Controlled Pressure Supply †

Paolo Righettini *, Roberto Strada, Filippo Cortinovis, Jasmine Santinelli and Federico Tabaldi

Department of Engineering and Applied Sciences, University of Bergamo, Viale Marconi 5, 24044 Dalmine, BG, Italy; roberto.strada@unibg.it (R.S.); filippo.cortinovis@unibg.it (F.C.); jasmine.santinelli@unibg.it (J.S.); federico.tabaldi@unibg.it (F.T.)

* Correspondence: paolo.righettini@unibg.it

† This paper is an extended version of our paper published in Righettini, P., Strada, R., Cortinovis, F., Santinelli, J. (2025). New Management Strategy for a Significant Reduction of the Impact on CO_2 Footprint of Hydraulic Actuators. In Proceedings of the 3rd IFToMM Workshop for Sustainable Development Goals (I4SDG), held in Villa San Giovanni, Italy, on 9–11 June 2025; Volume 179.

Abstract

Energy efficiency and sustainability are core issues in the modern design and management of industrial machinery and plants. These concerns are reflected and reinforced by the Sustainable Development Goal 9 of the United Nations (SDG9), "Industry, innovation and infrastructure", which enshrines efficiency and optimized energy use as key features of sustainable production systems. As the engineering of industrial machinery reorients itself towards energy sustainability, attention is naturally shifting to actuators, since these components unavoidably waste part of the considerable amount of energy they absorb to execute their functions. Hydraulic actuation systems, while uniquely suited to heavy-duty applications, are particularly affected by poor energy conversion efficiency, in part due to their intrinsic properties but also because of outdated yet still common industrial practices. Consequently, for this actuation technology, there are wide margins for improvement in terms of energy waste reduction and increased environmental sustainability. This paper, therefore, investigates new applications for a management and control method conceived by the authors to drastically and systematically reduce the energy consumption of hydraulic actuators. The method is easily retrofittable to existing plants, being based on the unconventional and non-invasive deployment of a continuous-control electrohydraulic valve (CCEV) to control the supply pressure, whose required value is estimated according to the instantaneous load demands. Through the simulation of several industrial processes characterized by process parameters of varying orders of magnitude, this paper demonstrates that this innovative use of a CCEV for supply pressure regulation is an effective and widely applicable solution for energy savings and CO_2 footprint reduction in production systems that rely on hydraulic servo axes.

Keywords: SDG9; carbon footprint reduction; energy efficiency optimization; hydraulic actuators; hydraulic servo and servo-proportional valves

Check for updates

Academic Editor: Zheng Chen

Received: 31 March 2026
Revised: 24 April 2026
Accepted: 26 April 2026
Published: 1 May 2026

Copyright: © 2026 by the authors. Licensee MDPI, Basel, Switzerland. This article is an open access article distributed under the terms and conditions of the Creative Commons Attribution (CC BY) license.

1. Introduction

The pursuit of energy sustainability, in terms of the minimization of energy consumption and CO_2 footprint reduction, plays a fundamental role in contemporary guidelines for

the design and management of industrial machinery and plants. Its importance is highlighted by the Sustainable Development Goal 9 of the United Nations (SDG9) "Industry, innovation and infrastructure" [1], according to which efficient and optimized energy use is a cornerstone of sustainable production systems. This trend is further attested by the growing scientific literature in which sustainability and energy efficiency are common threads in the design of different kinds of systems.

At the systemic level, ref. [2] addresses design approaches oriented towards the sustainability of production plants, while [3] reviews the sustainability concept in cellular manufacturing systems; in [4], the application of Model-Based System Engineering to smart sustainable factories is investigated. Other papers focus on energy efficiency and sustainability of specific components of the overall production system; ref. [5], for example, deals with the sustainability of reconfigurable machines, while [6] addresses the energy efficiency of robotic systems. The design of mechatronic systems is considered in [7], while [8] focuses specifically on linear electromechanical actuators. Among more recent works, ref. [9] analyzes the interplay between industry 4.0 and the circular economy for sustainability, while [10] reviews the links between industry 5.0 and sustainability.

In industrial systems, actuators are the main devices that absorb energy from the primary source to realize the specific function which the machine or plant is designed for. The absorbed energy is thus directed to the production of goods or, more generally, to the execution of specific operations within an integrated production process; in this context, energy is wasted primarily due to the less-than-ideal energy conversion efficiency of the actuators. Energy losses are an especially pressing issue wherever hydraulic actuators are used. Indeed, the motion control of hydraulic servo axes is intrinsically dissipative, as it is fundamentally based on the intentional throttling of the pressurized fluid that powers the actuator and on its partial redirection towards an unpressurized reservoir. The magnitude of these losses typically dwarfs the unavoidable dissipation associated with leakages [11] and distributed or localized pressure drops across the several components of the hydraulic circuit. Hence, in order to enhance sustainability of hydraulically actuated systems, improved management and control methods are of fundamental importance.

Many contributions concerning methods to reduce the energy waste of hydraulic actuators can be found in the literature but mostly concern solutions for specific application cases that do not have general validity and are not implementable in all kinds of systems; some examples of ad hoc approaches include [12], in which the application of a direct-driven hydraulics unit for an industrial high load lifting system is studied; Refs. [13,14] propose solutions for energy efficiency specifically tailored to hydraulic presses. The field of industrial presses is addressed also by many other authors: ref. [15] proposes the use of a multi-stage pressure system for a fine blanking press, while [16] details a metering valve-based configuration and a servo pump control to reduce energy waste in the leveling system in a large-size forming press. In [17], a system composed of multiple motor pumps and a supercharger–accumulator is proposed on a forging press, whereas in [18], the Industrial Internet of Things is used to perform an energy audit on a hydraulic press and so to acquire data for the control of a variable speed drive. Ref. [19] proposes an electromechanical–hydraulic model of a forging press for the evaluation of energy consumption in the different components; ref. [20], finally, describes the specific reconfiguration of a press and of its associated hydraulic circuit to reduce energy losses. Other works concern hydraulically actuated ground vehicles: a seminal work on the displacement control of rotary and differential linear hydraulic actuators in mobile machines is presented in [21], with the same line of investigation being further pursued in [22,23]; Refs. [24,25] review the main techniques used for energy savings in hydraulic excavators. Also, in [26,27], an excavator is considered; ref. [26] analyzes the powertrain and energy management strategies for such

vehicles, while [27] proposes the use of an electric–hydraulic system for energy recovery. Other examples of all-terrain vehicles considered in the literature are [28–30]; Refs. [28,29] propose energy-saving solutions based on specific energy-saving controllers or on new regenerative configurations; ref. [30] refers to a hydraulic fracturing vehicle on which a power consumption model is developed to predict efficiency of power elements. Other works can be found in the literature regarding other kinds of applications; for instance, ref. [31] concerns a lifting system on which a typical multi-valve configuration is compared to an electro-hydraulic drive in terms of energy consumption; ref. [32] discusses a robotic system where a two-level pressure system is considered to enhance the energy efficiency; and in [33], the redundant degrees of freedom of a manipulator are used to optimize energy consumption. Other more general works include [34], which reviews the innovations in energy efficiency in different sectors, and [35], which proposes a new circuit configuration for energy saving in an electro-hydraulic actuator without referencing particular applications. The largest portion of the reviewed scientific literature therefore concerns solutions engineered for specific application cases, without addressing applicability to a wide range of hydraulic systems. Furthermore, the implementation of such solutions is characterized by a large impact on the configuration of existing systems, as extensive modifications are required.

Within this context, the authors of this paper have conceived a new systematic methodology, whose feasibility has already been studied in a previous paper [36]; a setup for its experimental validation is also being studied [37]. The proposed approach is based on an estimate of the supply pressure required by the system to properly perform the desired work cycle according to the acting loads, and on an innovative, unconventional use of a continuous-control electrohydraulic valve (CCEV), an umbrella term covering servo, servo–proportional and proportional valves. Unlike the CCEV generally associated with hydraulic actuators for proportional directional control purposes, this additional valve is used within a pressure control system that guarantees the proper time-varying supply pressure by discharging as needed the excess flow rate. A similar technique for pressure regulation can be found in [38,39], where a control valve is used to vary the force applied by a hydraulic actuator on a semi-active friction damper. In the proposed methodology, on the other hand, pressure regulation is not used for force control but rather to reduce energy waste by decreasing the pressure drop towards the reservoir and by shifting the operating point of the actuator control valve towards a less dissipative regime.

In [36], the valve-based control technique placed emphasis on the use of servo valves to maximize the pressure control responsiveness; in this paper, on the other hand, the use of functionally equivalent valves is also evaluated: despite their different characteristics, other types of CCEV are also shown to be capable of playing similar roles in the achievement of high energy savings. Indeed, while servo valves guarantee higher control bandwidths, servo–proportional and proportional ones are typically available in a much wider size range, facilitating their introduction in larger plants.

This article is a revised and expanded version of a paper entitled "New Management Strategy for a Significant Reduction of the Impact on CO_2 Footprint of Hydraulic Actuators" [40], which was presented at the I4SDG 2025 Conference, Villa San Giovanni, Italy, 9–12 June 2025. This paper studies the application of the proposed supply pressure control method to simulated industrial application cases characterized by process parameters distributed across different orders of magnitude. In all these cases, the novel use of a continuous-control electrohydraulic valve as a device for pressure control is shown to be a scalable and highly effective solution for the reduction of energy consumption in hydraulic servo axis systems, which leads to a significant carbon footprint reduction. Notably, the proposed solution can be easily retrofitted to existing hydraulic plants, with

no change required other than the installation of an additional and suitably sized CCEV on the supply line.

2. Methods

The core subsystems of hydraulically actuated machinery treated in this paper are the hydraulic actuation units, composed of a linear actuator and the associated CCEV, which is used for motion control purposes. The control valve is interposed between the actuator and the hydraulic power supply system; the latter is traditionally set up in a Constant Flow Constant Pressure (CFCP) configuration, relying on a fixed-displacement pump and a constant-speed motor.

This architecture, where the supply pressure and flow rate are constant, provides non-adjustable hydraulic power generation and therefore entails maximum energy requirement. In this configuration, in fact, the flow and pressure at the pump outlet must be individually higher than the peak ones needed by the load. The first request is essentially kinematic and is strongly related to the peak velocity to be attained during the work cycle. The second is dynamic and depends on the kind of loads that the actuator should overcome. As a result, during the entire working cycle, the absorbed power is higher—in some portions significantly so—than the instantaneously needed one. To substantially mitigate this issue, the methodology introduced by the authors [36] employs a Controlled Hydraulic Power Supply (CHPS) to adjust the power made available to the actuator.

As illustrated in Figure 1, one of the implementations of the CHPS there proposed relies on a CCEV that regulates the supply pressure through the discharge of the excess flow rate provided by a fixed displacement and fixed speed pump unit. The figure, in particular, represents in black the following hydraulic elements:

- The actuator, with its chambers A and B, its position x and its velocity $\dot{x}$;
- The mechanical load F_{ml} applied to the piston;
- The actuator control valve;
- The pressure control valve;
- A manually regulated relief valve that guarantees safety;
- The constant-speed prime mover and the fixed displacement pump.

The relevant gauge pressures P_T at the reservoir, P_A in chamber A, P_B in chamber B and P_S at the pump outlet are also represented at the relevant nodes of the hydraulic circuit.

The required sensors and algorithmic components are represented in cyan; the latter are:

- The motion setpoint generator;
- The motion controller, which determines the opening of the actuator CCEV;
- The pressure controller, which determines the opening of the pressure CCEV;
- The Hydraulic Efficiency Optimizer (HEO), which generates the pressure setpoint;
- The Hydraulic Actuator Load Estimator (HALE), which supplies the HEO with an estimate of the mechanical load.

This specific CHPS implementation is the one that requires the fewest and least expensive modifications to existing plants that currently adopt the traditional CFCP configuration, as it does not need alterations to the motor–pump functional group. The use of a CCEV to control the supply pressure has one further advantage with respect to the other possible solutions, namely, the achievement of bandwidths (depending on the specific valve type) that typically exceed those of, e.g., variable displacement pumps; this property makes it suitable for use in applications characterized by markedly dynamic loading conditions.

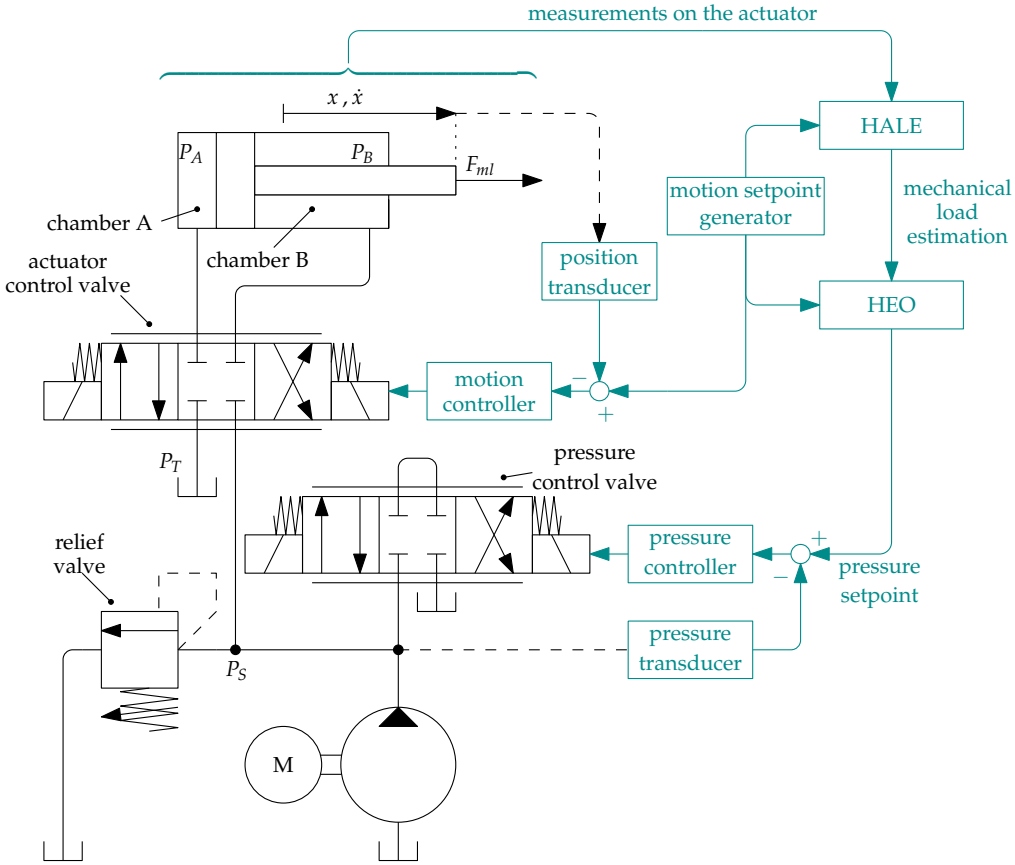


Figure 1. Schematic representation of the hydraulic system inclusive of the continuous-control electrohydraulic valve used for pressure regulation.

The pressure regulation is achieved through a control loop that determines the opening of the relief CCEV, comparing the measured supply pressure with a suitable setpoint. Such a setpoint is generated according to the dynamic model of the actuator [41–44], to the load requests, and to the need of minimizing energy consumption without compromising motion control performances. Focusing without loss of generality on a double-rod linear actuator, for the purpose of defining the supply pressure setpoint, the following physical model of the actuation unit is adopted:

$$P_L = P_A - P_B = -\frac{F_{ml}}{A} \tag{1}$$

$$Q_L = C_t P_L + A\dot{x} \tag{2}$$

$$Q_L = K H_{ACV} \sqrt{P_S - \text{sign}(H_{ACV}) P_L}\,. \tag{3}$$

Equation (1) expresses the mechanical equilibrium of the piston; there, P_L indicates the line pressure, i.e., the difference between the gauge pressures P_A and P_B; A is the effective piston area, while F_{ml} is the mechanical load applied to the cylinder, inclusive of all forces (external, inertial and dissipative).

Equation (2) expresses the relationship between the piston velocity $\dot{x}$ and the line volumetric flow Q_L, which, although primarily governed by the area A, involves also the leakage coefficient C_t and the line pressure P_L. Finally, Equation (3) describes the hydraulic behavior of the actuator CCEV: H_{ACV} is its instantaneous normalized opening (varying in the range $[-1\,,1]$, and connecting chamber A to the reservoir if negative), K its characteristic coefficient (obtainable from the manufacturer's data sheet), and P_S the supply pressure.

Rearranging Equation (3) and using (1), the supply pressure can be expressed as follows:

$$P_S = \left(\frac{Q_L}{KH_{ACV}}\right)^2 + \text{sign}(H_{ACV})P_L\,, \tag{4}$$

where the first term on the right-hand side, under the assumption of symmetrical valve ways, represents the total pressure drop P_V across the actuator control valve. From Equation (4), it appears that a double benefit is achieved through the maximization of $|H_{ACV}|$: first of all, the pressure drop across the actuator control valve is reduced; second, P_S also decreases. Less wasted energy is thus associated with any excess flow rate sent to the reservoir through the relief CCEV.

Outside of dwell phases, the equality $\text{sign}(H_{ACV}) = \text{sign}(\dot{x})$ holds; substituting it into (4), it may be seen that when the mechanical load has a driving action (i.e., for $W_L = F_{ml}\dot{x} > 0$), there is a risk of negative P_S for excessive values of $|F_{ml}|$. An even more pressing risk is that of suction in the filling chamber, whose pressure is lower than P_S due to the drop across the position control valve way.

In greater detail, assuming $\text{sign}(H_{ACV}) = 1$ and symmetrical valve ways, the following equations may be derived:

$$P_V = 2(P_S - P_A) = 2(P_B - P_T) = 2P_B \tag{5}$$

$$P_B = P_A - P_L \tag{6}$$

$$P_A = P_S - \frac{P_V}{2} = \frac{P_V}{2} + P_L\,; \tag{7}$$

in Equation (5), the gauge pressure P_T is equal to zero, consistent with an unpressurized reservoir. Requiring then that $0 < P_A < P_S$, the following inequalities are obtained:

$$P_S > \frac{P_V}{2} \tag{8}$$

$$P_V > -2P_L\,. \tag{9}$$

A result identical to (8) can be obtained with symmetric reasoning applied to the case characterized by $\text{sign}(H_{ACV}) = -1$; on the contrary, the inequality analogous to (9) obtained in this alternative condition is $P_V > 2P_L$. To account for both cases, therefore, the following can be written:

$$P_V > -2\text{sign}(H_{ACV})P_L = -2\text{sign}(\dot{x})P_L\,. \tag{10}$$

t may be easily seen that for $W_L < 0$ both (8) and (10) are trivially satisfied and that consequently, sub-atmospheric pressure is not a risk regardless of the value of P_S and H_{ACV}. On the contrary, for $W_L > 0$, algebraic manipulation of (10) yields:

$$|H_{ACV}| < \frac{|Q_L|}{K}\sqrt{\frac{1}{2|P_L|}}\,. \tag{11}$$

To avoid suction in the filling chamber, then, (11) should be enforced together with (8). In light of the relationships above, there is no unique solution for H_{ACV} and P_S; rather, the two quantities should be properly related to each other and to the mechanical load F_{ml} using (4), (8) and (11). As conceptualized in [36], the strategy for the proper definition of the pressure setpoint involves two algorithmic modules, which in general admit a variety of possible implementations: the Hydraulic Actuator Load Estimator (HALE), which provides an estimate $\hat{F}_{ml}$ of F_{ml} (or equivalently an estimate $\hat{P}_L = -A^{-1}\hat{F}_{ml}$ of P_L), and the Hydraulic Efficiency Optimizer (HEO), which determines a suitable supply pressure setpoint $P_{S,sp}$

through the selection of a reference valve opening $H_{ACV,ref}$. To ensure robustness to model and load uncertainties, the opening of the actuator valve is not controlled in an open loop; yet, as P_S tracks $P_{S,sp}$, the actual value of H_{ACV} can be expected to be broadly similar to $H_{ACV,ref}$. The straightforward HEO implementation proposed in this work defines the absolute value of $H_{ACV,ref}$ as:

$$|H_{ACV,ref}| = \begin{cases} H^* & \text{for } \hat{F}_{ml}\dot{x}_{sp} \leq 0 \\ \min\left(H^*, \dfrac{A|\dot{x}_{sp}|}{K}\sqrt{\dfrac{1}{2|\hat{P}_L|}}\right) & \text{for } \hat{F}_{ml}\dot{x}_{sp} > 0\,. \end{cases} \tag{12}$$

In (12), the product between A and the absolute value of the setpoint velocity $|\dot{x}_{sp}|$ provides a useful estimate of the modulus $|Q_L|$ of the line volumetric flow. Crucially, the positive constant H^* should be high enough to ensure sizable energy savings but still reasonably far from unity to provide a saturation-free margin of action for the position control loop. Considering also the static case in which the piston is kinematically at rest, the pressure setpoint defined by the proposed HEO implementation is:

$$P_{S,sp} = \begin{cases} |\hat{P}_L| + P_{S,sp,0} & \text{for } \dot{x}_{sp} = 0 \\ \left(\dfrac{A\dot{x}_{sp}}{K|H_{ACV,ref}|}\right)^2 + \text{sign}(\dot{x}_{sp})\hat{P}_L + P_{S,sp,0} & \text{otherwise}\,, \end{cases} \tag{13}$$

where $P_{S,sp,0}$ is a small positive constant introduced to improve robustness with respect to uncertainties concerning the load and the pressure setpoint tracking performance. For completeness, including the static case, the sign of $H_{ACV,ref}$ is defined by the HEO algorithm as:

$$\text{sign}\left(H_{ACV,ref}\right) = \begin{cases} 1 & \text{for } \dot{x}_{sp} > 0 \\ -1 & \text{for } \dot{x}_{sp} < 0 \\ \text{sign}\left(\hat{P}_L\right) & \text{for } \dot{x}_{sp} = 0\,, \end{cases} \tag{14}$$

where the convention $\text{sign}(0) = 0$ is adopted.

As already remarked upon, several implementations for the HALE module are also possible. In a repetitive industrial cycle, $\hat{P}_L$ or equivalently $\hat{F}_{ml}$ may be estimated from existing data; other possibilities are measurement-based online estimations or suitable parametric mathematical models. In the following discussion, the mechanical load is assumed to behave as:

$$P_L A = -F_{ml} = m\ddot{x} + c\dot{x} - F_{ext}\,, \tag{15}$$

where F_{ext} is a known external load, inclusive of gravitational actions if appropriate, m and $\ddot{x}$ are, respectively, the overall mass and the acceleration of the piston, and c is the viscous friction coefficient. Accordingly, under the assumption of already determined mass and friction parameters, the HALE estimator is simply:

$$\hat{F}_{ml} = F_{ext} - m\ddot{x}_{sp} - c\dot{x}_{sp}\,, \tag{16}$$

where $\ddot{x}_{sp}$ is the piston acceleration setpoint.

Without loss of generality, this simple implementation has been used for the simulations presented in the following section. More complete ones would include online or offline mass, friction and external load identification strategies, or approaches based directly on pressure measurements in the actuator chambers. Online algorithms have the benefit of adaptability to non-cyclical conditions; while their implementation requires a careful evaluation of their computational cost, the option of relying on direct pressure

measurements suggests that the achievement of relatively low complexity and good compatibility with real-time requirements is possible. Robustness against inaccuracies in the HALE module outputs, and against pressure tracking errors, is guaranteed by the position control loop, which remains an important part of the proposed architecture specifically for this reason. In particular, if P_S does not accurately match the load requests, the position control loop will adjust the opening of the actuator valve, whose value will deviate from $H_{ACV,ref}$; to reduce the likelihood of saturation of such adjustments, the value of $P_{S,sp,0}$ can be increased and H^* can be reduced; this further increases robustness at the cost of reduced energy efficiency.

3. Results

In order to assess the feasibility of pressure regulation based on the use of a continuous-control electrohydraulic valve, simulations are performed on real industrial cases; the considered applications concern in particular hydraulic presses executing the following operations:

- Forging;
- Self-piercing riveting;
- Hot stamping.

Numerical simulations are performed using MathWorks Simscape, thus testing the proposed strategy on numerical models more sophisticated than those used for the computation of $P_{S,sp}$.

In particular, the following effects, neglected during the definition of the pressure setpoint, are considered: compressibility of the fluid in the actuator chambers; limited bandwidth of the control valves; and fluid expansion effects due to the pressure drops across the valves. Pipeline effects are neglected but could be considered within simulations of cases where more detailed information concerning the plant configuration is available.

The position of the actuator and the supply pressure are controlled, respectively, with Proportional-Derivative (PD) and Proportional (P) regulators. The controller parameters are empirically tuned for each case to satisfy the dynamic characteristics of the position and pressure setpoints, avoiding excessively aggressive gains that tend to induce oscillations in the motion of the system. The reported results are:

- The already described $\hat{F}_{ml}$, $P_{S,sp}$, P_S, $\dot{x}_{sp}$ and $\dot{x}$;
- The actual position x and the setpoint x_{sp};
- The flow rate towards the filling chamber of the actuator Q_S (coinciding with Q_L in the absence of compressibility effects) and the setpoint $Q_{S,sp} = A\dot{x}_{sp}$;
- The opening of the actuator CCEV H_{ACV} and of the relief CCEV H_{PCV};
- The input hydraulic energy E_{in}, the energy wasted across the actuator control valve E_{ACV}, and the energy lost across the relief CCEV E_{PCV}.

3.1. Forging Press Application Case

The forging application case considered refers to a 120-ton forging press; the relevant work cycle, drawn from [45,46], is represented in Figure 2 both in terms of forging force (i.e., the external force acting on the actuator) and of the upper die displacement, which is directly actuated by the piston.

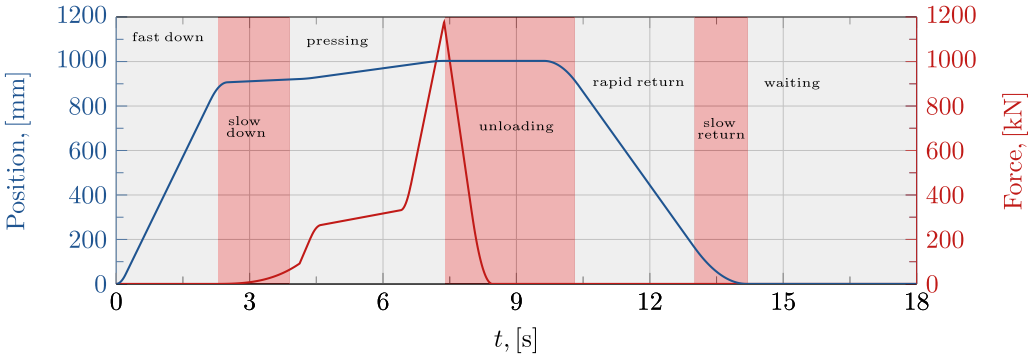


Figure 2. Forging work cycle: forging force exerted on the workpiece and upper die displacement.

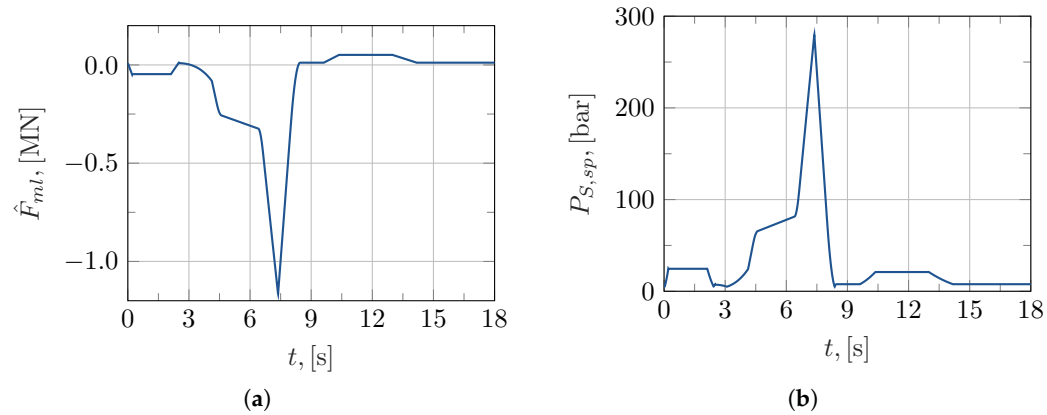
As also reported in the figure, the work cycle is composed of seven phases:

- *Rapid down*: the upper die rapidly moves towards the billet to be worked;
- *Slow down*: the upper die approaches the billet;
- *Pressing*: the forging operation occurs;
- *Unloading*: the forging load decreases;
- *Rapid return*: the upper die rapidly moves towards its initial position;
- *Slow return*: the upper die decreases its velocity while approaching its initial position;
- *Waiting*: the upper die remains stationary while waiting for the next cycle.

The main components of the hydraulic circuit are:

- A four-way proportional valve for motion control (Bosch-Rexroth 4WRLD35E11500, nominal flow rate 1500 L min^{-1});
- A four-way proportional valve for pressure control (Bosch-Rexroth 4WRLD35E11500, nominal flow rate 1500 L min^{-1});
- A double-acting, double-rod hydraulic actuator (Bosch-Rexroth CGH3MT4/320/220/1250, 320 mm piston diameter, 220 mm rod diameter, 1250 mm stroke).

The bandwidth for the two control valves is estimated from the manufacturer's data sheet and set to 5 Hz. The simulation results are reported in Figures 3–5; Figure 3 depicts the outputs of the HALE and HEO modules, namely, the mechanical load estimate and the reference supply pressure.



(**a**) (**b**)

Figure 3. Forging application case: (**a**) estimated mechanical load force; (**b**) reference supply pressure.

The estimate of the mechanical load $\hat{F}_{ml}$ also includes the weight force, the inertial actions, and the viscous actions; for this application case, it is calculated according to Equation (16), where all the system parameters are supposed to be known. It should be noted that the sign of $\hat{F}_{ml}$ is considered positive if its direction corresponds to the actuator extending direction, i.e., towards the piece to be worked. Figure 3b shows the reference

supply pressure calculated according to Equation (13) with $H^* = 0.75$, which exhibits a strongly variable behavior with a high peak value. Figures 4 and 5 report the actual behavior of the system when the motion setpoint and the pressure setpoint are assigned. Figure 4a shows that the supply pressure and supply flow rate setpoints are followed very precisely except when the relief CCEV saturates its opening, as shown by the comparison with Figure 5a.

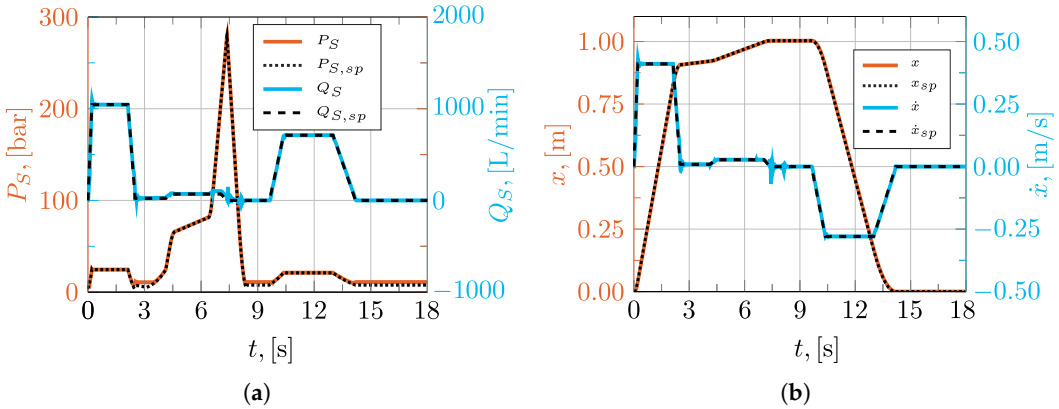


Figure 4. Forging application case: pressure and motion control; (**a**) supply pressure and supply flow rate setpoints ($Q_{S,sp}$, $P_{S,sp}$) and actual values (Q_S, P_S); (**b**) position and velocity setpoints (x_{sp}, $\dot{x}_{sp}$) and actual values (x, $\dot{x}$).

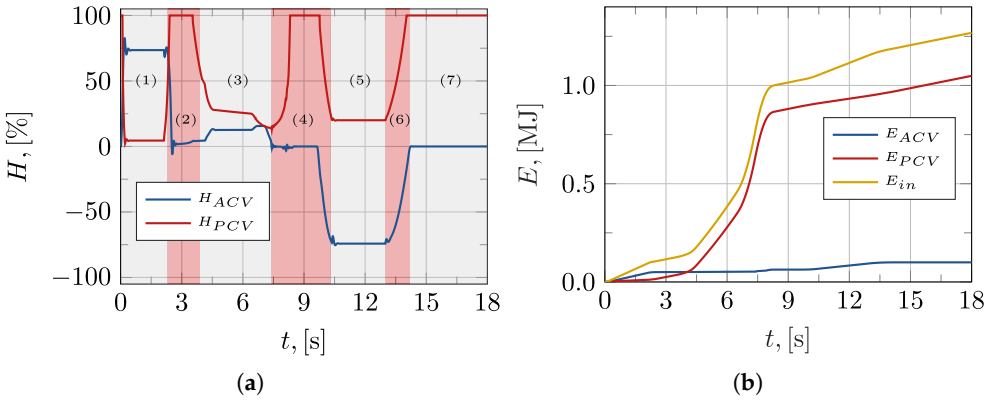


Figure 5. Forging application case: control valve openings and hydraulic energies; (**a**) openings of the actuator (H_{ACV}) and pressure (H_{PCV}) control valves; (**b**) input (E_{in}) and wasted hydraulic energies across pressure (E_{PCV}) and actuator (E_{ACV}) control valves.

The position and velocity setpoints are followed with very high accuracy, as shown in Figure 4b, except for small oscillations in the velocity response. Such an oscillation occurs, for example, around the 7.5 s mark, when the load reaches its maximum value, probably due to the fact that the fluid's compressibility has been considered in this simulation. Figure 5a depicts the actuator control valve opening, where labels (1)–(7) indicate the different work cycle phases; saturation does not occur, and when the piston moves, it works around $|H_{ACV}| = 0.75$, which corresponds to the value chosen for H^* in Equation (12). Moreover, considering also the graph of the relief CCEV opening, Figure 5a shows that during phase 1 of the work cycle ("rapid down"), the pressure control valve is nearly closed since only a very small amount of flow rate needs to be discharged, while the actuator valve works near $H_{ACV} = 0.75$ to guarantee the proper flow rate to the actuator. During phase 2 ("slow down"), the relief CCEV saturates because the velocity is very low, and therefore a large amount of flow rate generated by the pump unit has to be discharged. During this phase, the actuator control valve has a very small opening in order to guarantee the

proper tracking of the low speed reference. Also during phase 3 ("pressing"), the actuator control valve has a modest opening because of the low actuator speed, but also the relief CCEV is almost closed because high pressure is required to generate high working forces. In phase 4 ("unloading"), the actuator is at rest; hence, its control valve opening equals zero; on the contrary, the relief CCEV saturates because the whole pump flow rate has to be discharged through it and no working force is required. In phase 5 ("rapid return"), the actuator control valve has a negative opening to reverse the motion at the proper speed, while the relief CCEV has a small opening because almost all the flow rate is required by the actuator. During phase 6 ("slow return"), the actuator control valve obviously decreases its opening while the relief CCEV increases its own to allow the discharge of the excess flow rate. Finally, in phase 7 ("waiting"), the required velocity and force are zero, so the actuator control valve is closed and the relief CCEV fully opens in order to discharge all the pump flow rate. Figure 5b shows the graph of the total hydraulic input energy (E_{in}) and of the energy wasted across either the actuator control valve (E_{ACV}) or the relief CCEV (E_{PCV}). The figure shows that E_{PCV} is a large fraction of E_{in}; this occurs because for a significant portion of the work cycle, the flow rate required by the actuator is very low or zero; this causes the pump flow rate to entirely, or almost entirely, discharge through the relief CCEV. Moreover, the actual value of the supply pressure is always higher than the atmospheric one, i.e., the pressure drop across the relief CCEV is never zero. In addition, during the "pressing" phase, when the actuator flow rate is very low, the supply pressure must concurrently reach high values; this results in high power waste due to the discharge of large flow rate at a high pressure drop.

3.2. Self-Piercing Riveting Application Case

Self-piercing riveting is a process for joining metal-sheet stacks; the rivet, driven by a punch, pierces the top sheet, flares into the bottom sheet and clamps the two together, producing the joint [47,48]. The process is widely used in the automotive industry and is composed of different phases; the overall work cycle, drawn from [47,48], is depicted in Figure 6, which represents both the punch displacement and the load force. It should be noted that the riveting process is characterized by a load force and a cycle time that are two orders of magnitude lower than the previously analyzed application case. The different phases characterizing the riveting process are:

- *Approaching*: the punch approaches the rivet at high speed and, before touching it, decelerates;
- *Piercing*: the punch makes contact with the rivet and so the load force starts increasing; during this phase, the punch speed also increases;
- *Flaring*: the punch speed decreases and remains constant during the phase, while the load force has an approximately linear increase up to a maximum value corresponding to the rivet clamping;
- *Return*: during this phase, the punch returns back to its initial position at high speed; the load force is null;
- *Waiting*: the system is waiting for the next work cycle.

Since in this application case the force is significantly lower than that of the forging work cycle, the main components of the hydraulic circuit considered to perform the simulations have been downsized accordingly; these are:

- A four-way servo valve for motion control (Bosch-Rexroth 4WS2EM62X15 series, 15 L min^{-1} nominal flow);
- A four-way servo valve for pressure control (Bosch-Rexroth 4WS2EM62X20 series 20 L min^{-1} nominal flow);

- A hydraulic actuator (Bosch-Rexroth CGH2MT4/80/50/100, double-acting, double-rod cylinder with 80 mm piston diameter, 50 mm rod diameter and 100 mm stroke).

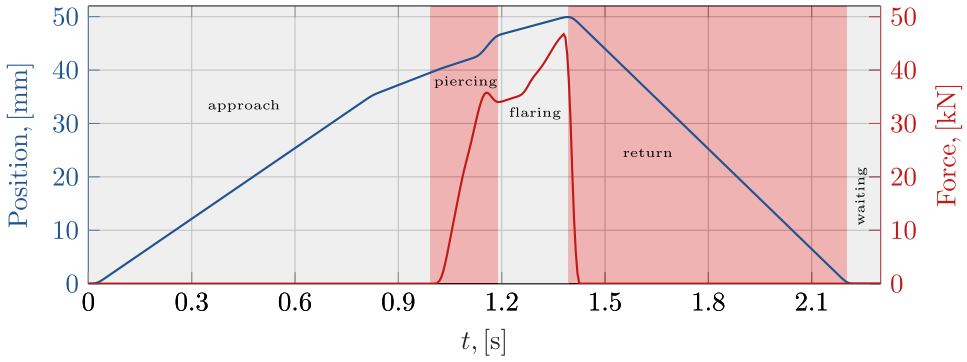
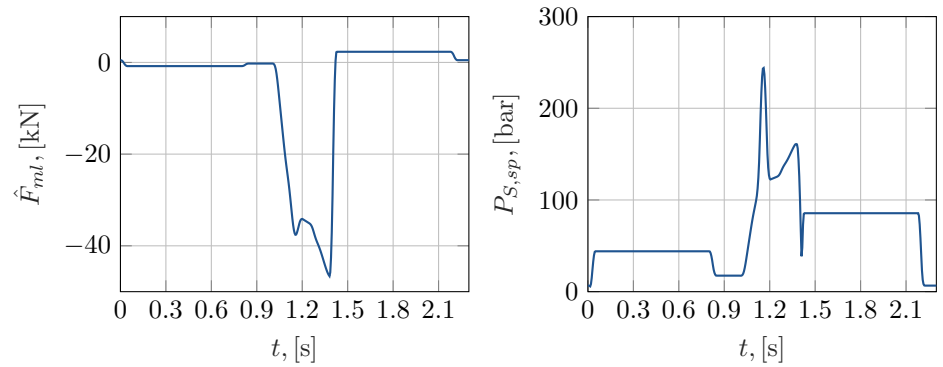


Figure 6. Riveting work cycle: punch displacement and force exerted on the rivet.

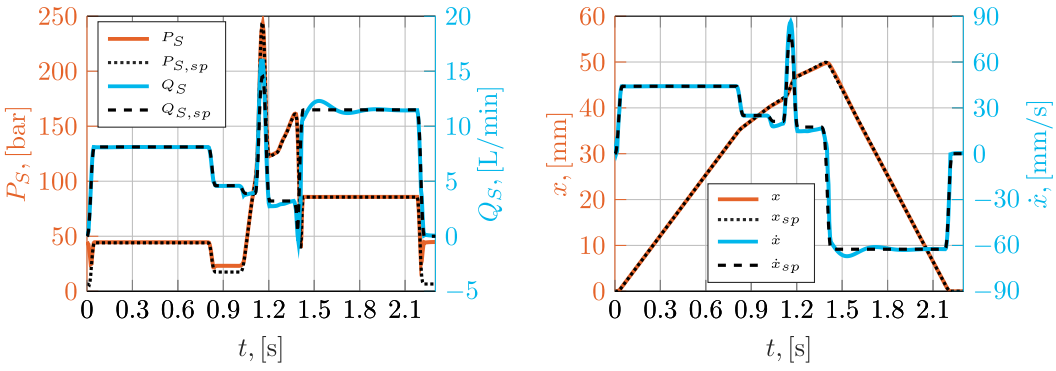
The bandwidth for the two servo valves is set to 100 Hz, consistent with the manufacturer's data. Figures 7–9 depict the simulation results; Figure 7 in particular shows the graphs of the mechanical load estimate and the reference supply pressure, i.e., the outputs of the HALE and HEO modules. Also for the riveting application case, the mechanical load estimate includes the weight and the inertial and the viscous forces, and it is evaluated according to Equation (16), assuming that all the system parameters are known. The force is considered positive if directed towards the parts to be riveted. The behavior of the reference supply pressure, calculated considering $H^* = 0.75$, is shown in Figure 7b. Its variations reflect those of the required velocity and the estimated load force (or equivalently of the required flow rate Q_L and load pressure P_L). Such quantities contribute to the definition of the reference supply pressure according to Equation (13); as an example, around 0.3 s and in the range 0.4 s to 0.6 s, the reference supply pressure reproduces the behavior of the estimated load force, while at the beginning of the work cycle, between 0.3 s and 0.4 s and from 0.6 s to the end time, the shape is very similar to that of the velocity graph. Figure 8 shows the simulation results in terms of supply pressure, flow rate Q_S towards the actuator, piston position and velocity. In particular, Figure 8a depicts the setpoint and the actual values of the supply pressure P_S and the supply flow rate Q_S; the comparison of the graphs shows a very good match between setpoints and actual values. Small differences between desired and actual supply pressure occur within the time ranges in which very small values are required, as, for example, around 0.15 s. There, the actual pressure remains higher due to the relief servo valve reaching saturation, i.e., its maximum opening, in flow conditions that imply a pressure drop greater than the setpoint value. As regards the supply flow rate, a small error is evident between 0.6 s and 0.8 s; this behavior could be due to the opening of the actuator servo valve, which gradually increases, and of the relief servo valve, which correspondingly decreases, as shown in Figure 9a, where the labels (1)–(5) indicate the different work cycle phases; this behavior can be attributed to the performance of the control system. Figure 8b depicts piston position and velocity; the comparison between the setpoints and the actual values shows also in this case a very good correspondence. Small differences can be noted for the velocity, mainly between 0.6 s and 0.8 s; a matching behavior, attributable to the control system, can be seen in the discharged flow rate. Such a velocity error does not in any way affect the riveting process, since it occurs during the return phase. Figure 9a depicts the non-dimensional opening of the servo valves; in particular, except during the time ranges characterized by very small velocities, the actuator servo valve works around an opening equal to 0.75, corresponding to the H^* value considered in Equation (12) for the calculation of the supply pressure setpoint. As regards the relief servo valve opening, it saturates whenever the velocity of the actuator is very

low; as the load flow rate is low as well, the amount of pump flow rate to be discharged through the relief servo valve is high. This occurs both at the beginning and at the end of phase 1 ("approach"); in the middle range of the phase, the velocity and the supply pressure setpoint increase, leading to an increase in the actuator servo valve opening and a decrease in the servo-relief one. During phase 2 ("piercing"), the valve openings have a sudden change concurrent with the increase in the supply pressure setpoint and of the piston velocity; this occurs around 0.35 s. In phase 3 ("flaring"), the piston velocity remains constant and the setpoint supply pressure has an approximately linear increase, leading to a consequent servo valve opening behavior. In phase 4 ("return"), the relief servo valve opening decreases and that of the actuator servo valve increases; this is due, on one hand, to the increase in the velocity and so of the load flow rate, and, on the other hand, to the supply pressure setpoint. As a matter of fact, a large opening of the actuator servo valve guarantees the piston velocity, while a small opening of the relief servo valve allows the required supply pressure and limits the discharged flow rate. Phase 5 is the waiting phase, where the relief servo valve saturates and the actuator servo valve is closed because the piston remains stationary and the whole pump flow rate is discharged through the relief servo valve. Finally, Figure 9b depicts the graph of the total hydraulic input energy E_{in}, of the wasted energy across the actuator servo valve E_{ACV} and across the relief servo valve E_{PCV}. Also, in this case, E_{PCV} is a significant fraction of E_{in}; unlike the previous case, the energy wasted across the actuator servo valve E_{ACV} is also quite significant. This occurs because in this case, for most of the work cycle, the piston is in motion.



(**a**) (**b**)

Figure 7. Riveting application case: (**a**) estimated mechanical load force; (**b**) reference supply pressure.



(**a**) (**b**)

Figure 8. Riveting application case: pressure and motion control; (**a**) supply pressure and supply flow rate setpoints ($Q_{S,sp}$, $P_{S,sp}$) and actual values (Q_S, P_S); (**b**) position and velocity setpoints (x_{sp}, $\dot{x}_{sp}$) and actual values (x, $\dot{x}$).

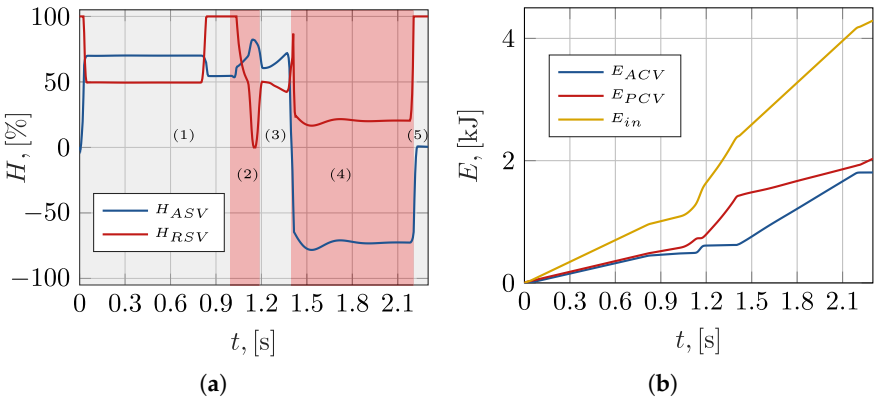


Figure 9. Riveting application case: servo valve openings and hydraulic energies; (**a**) actuator servo valve (H_{ACV}) and relief servo valve (H_{PCV}) openings; (**b**) input (E_{in}) and wasted hydraulic energies across pressure (E_{PCV}) and actuator (E_{ACV}) control valve.

3.3. Hot Stamping Application Case

Hot stamping is a forming technology widely used in the automotive, aerospace, and industrial equipment manufacturing sectors. The forming process as a whole is characterized by different main sequential steps [49] that make it possible to form a metal sheet according to the shape of a specific die set. The press work cycle, drawn from [49], is depicted in Figure 10; it should be noted that this application case is characterized by a peak force that is substantially higher compared to the previously analyzed cases and that moreover must be sustained for a longer time of about 30 s.

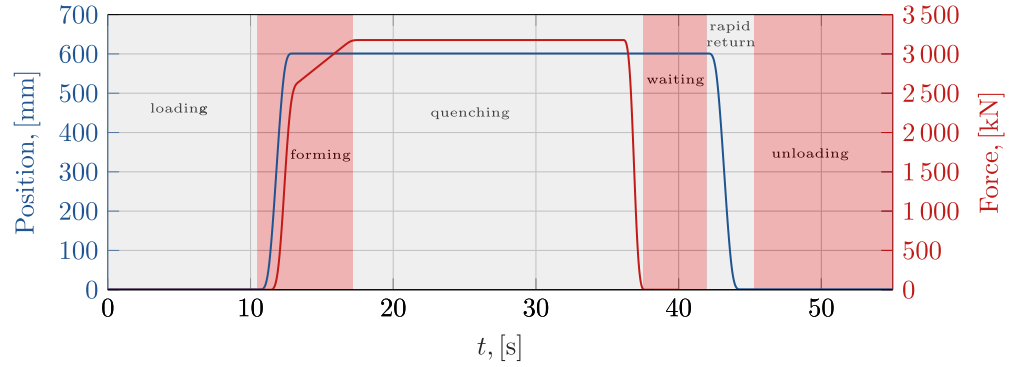


Figure 10. Hot stamping work cycle: upper die displacement and hot stamping force on the workpiece.

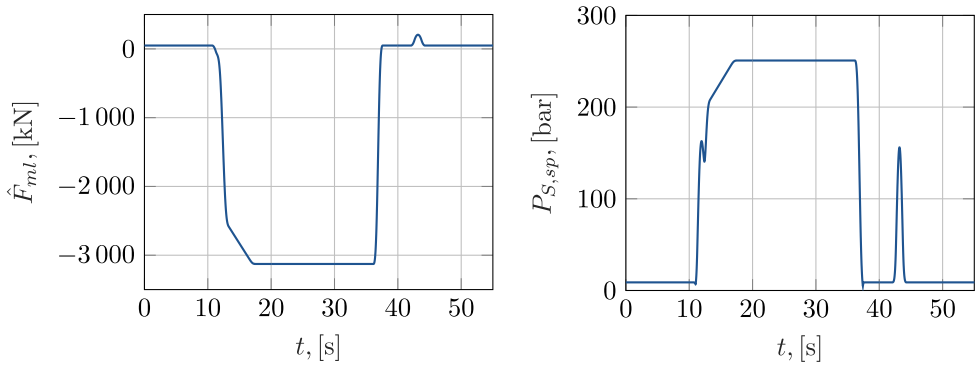
The work cycle is composed of six phases:

- *Loading*: the die is fully open while the unformed metal sheet is being loaded;
- *Forming*: during this phase the ram rapidly approaches the metal sheet; once in contact with it, the forming operation occurs;
- *Quenching*: the force is kept constant at its maximum value and the die remains closed; during this phase, the formed part is hardened;
- *Waiting*: the die is kept closed with almost zero force applied; the press is waiting for unloading operation to start;
- *Rapid return*: the ram rapidly moves back to its initial position, opening the die;
- *Unloading*: during this phase, the press is fully open and is waiting for the formed part to be removed.

Due to the characteristics of the work cycle, the hydraulic components considered for the simulations are of larger size with respect to the ones considered for the riveting and also for the forging application case. These are:

- A four-way proportional valve for motion control (Bosch-Rexroth 4WRLE35, 1500 L min^{-1} nominal flow rate);
- A four-way proportional valve for pressure control (Bosch-Rexroth 4WRLE35, 1500 L min^{-1} nominal flow rate);
- Three double-acting, double-rod hydraulic actuators working in parallel (Bosch Rexroth CGH3MT4/320/220/750, 320 mm piston diameter, 220 mm rod diameter, 750 mm stroke).

Due to their larger size, the bandwidth for the two control valves is estimated to be 7 Hz. The simulation results are depicted in Figures 11–13. The estimated mechanical load force provided by the HALE module is represented in Figure 11a. Also for this application case, this force is calculated according to Equation (16), assuming that the load conditions are completely known. Therefore, the shape of the graph results from the contributions of the external, inertial and viscous forces; again, the sign of the force is positive if directed towards the part to be formed. The supply pressure setpoint provided by the HEO module is depicted in Figure 11b.



(**a**) (**b**)

Figure 11. Hot stamping application case: (**a**) estimated mechanical load force; (**b**) reference supply pressure.

Having been calculated with Equation (13), $P_{S,sp}$ clearly shows the contributions of the load pressure and flow rate. This can be seen also through a comparison with Figures 11a and 12b. Starting from the outputs of the HALE and HEO modules, and from the required piston motion, the simulation yields the results depicted in Figure 12a,b. Both figures show that the setpoints of the supply pressure P_S and of the supply flow rate Q_S are followed with high accuracy; an exception concerns the supply pressure in the time ranges at the beginning and at the end of the work cycle. These are periods in which the piston velocity is zero, leading to the discharge of the whole pump output through the relief proportional valve. Moreover, since the estimated load force is also zero, the pressure setpoint equals the atmospheric pressure; the pressure control system consequently completely opens the relief proportional valve (see Figure 13a, where the labels (1)–(6) indicate the different work cycle phases) to satisfy these conditions. However, as saturation is reached, the supply pressure does not follow the setpoint because of the unavoidable pressure drop across the fully opened valve. On the contrary, when the piston starts moving, Figure 12a shows a decrease in the supply pressure because the flow rate to the actuator Q_S increases and so the amount of pump flow rate to be discharged is lower; this occurs briefly around the 11 s and 42 s marks. Focusing on the opening of the proportional valves depicted in Figure 13a, other considerations can be made. Whenever the piston velocity is null, the actuator control valve is kept closed to prevent supplying flow rate to the actuator itself. On the contrary, when the piston moves, the valve opens at 75%, corresponding to $H^* = 0.75$, that is, the

value considered in Equation (12). As regards the relief proportional valve, it saturates when the entire pump flow rate has to be discharged due to the fact that the piston is at rest and that the supply pressure setpoint equals the atmospheric one. Around 11 s and 42 s, the relief proportional valve opening decreases because the piston starts moving, requiring a flow rate, and at the same time the supply pressure setpoint increases. At 11 s, the supply pressure increases because of the working and inertial forces, while at 42 s the increase is due just to the inertial actions. The analysis of the results concludes with Figure 13b, where the different contributions to the wasted energy are reported. Unlike the previous cases, the wasted energy associated with the actuator control valve E_{ACV} is very low and can be considered negligible with respect to that of the relief proportional valve E_{PCV}. This is due to the fact that in the hot stamping work cycle, the piston remains stationary for long intervals in which the actuator control valve stays closed and consequently experiences no pressure drop. On the contrary, the energy wasted across the relief proportional valve is approximately equal to the overall hydraulic energy input; in fact, on one hand, when the actuator control valve is closed, the whole pump flow rate discharges through the relief proportional valve, on the other hand, a high working force, and so a high supply pressure, is required for a significant portion of the working cycle.

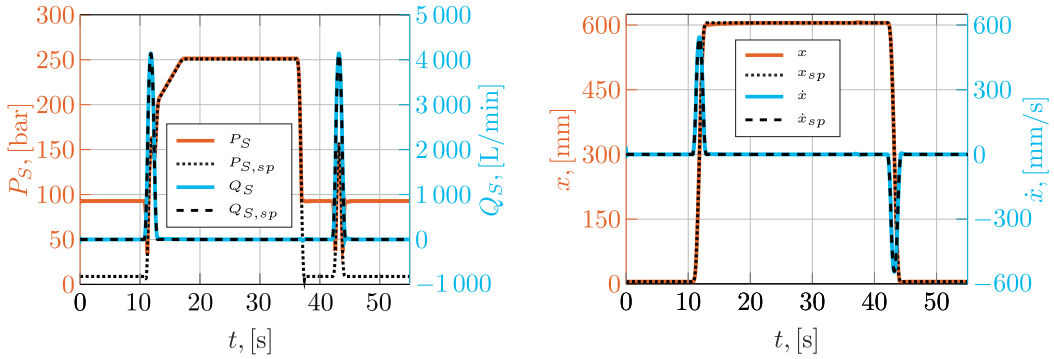


Figure 12. Hot stamping application case: pressure and motion control; (**a**) supply pressure and supply flow rate setpoints ($Q_{S,sp}$, $P_{S,sp}$) and actual values (Q_S, P_S); (**b**) position and velocity setpoints (x_{sp}, $\dot{x}_{sp}$) and actual values (x, $\dot{x}$).

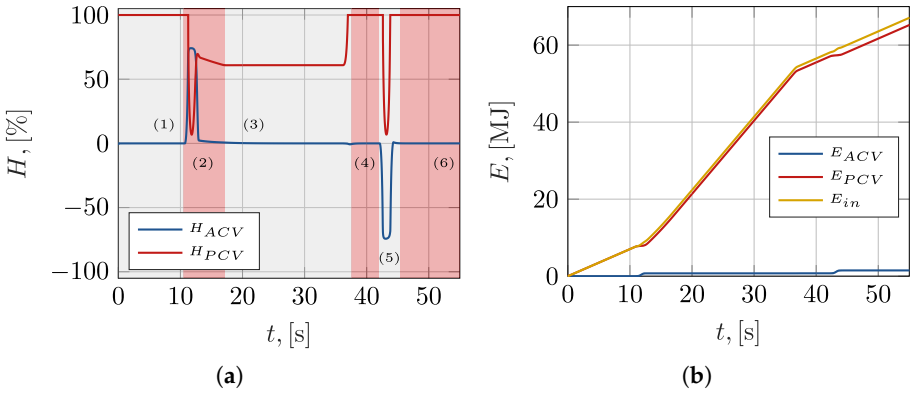


Figure 13. Hot stamping application case: control valve openings and hydraulic energies; (**a**) actuator control valve (H_{ACV}) and relief proportional valve (H_{PCV}) openings; (**b**) input (E_{in}) and wasted hydraulic energies across pressure (E_{PCV}) and actuator (E_{ACV}) control valves.

4. Discussion

In this section, the results are discussed, pointing out the energy wasted during the different operations with particular reference to the energy savings achieved in comparison

with the traditional CFCP method. According to this traditional method, the hydraulic power supply is not adjustable: the supply pressure and the pump flow rate are fixed. The considered fixed pump flow rate and constant supply pressure are different for each application case, having been chosen to be slightly in excess of the maximum work cycle requests. Their values are:

- *Forging*: pump flow rate $Q_{P,CFCP} = 1150\,\mathrm{L\,min^{-1}}$, supply pressure $P_S = 300\,\mathrm{bar}$, corresponding hydraulic input energy $E_{in,CFCP} = 10{,}350\,\mathrm{kJ/cycle}$;
- *Self-piercing riveting*: pump flow rate $Q_{P,CFCP} = 15.95\,\mathrm{L\,min^{-1}}$, supply pressure $P_S = 300\,\mathrm{bar}$, corresponding hydraulic input energy $E_{in,CFCP} = 18.37\,\mathrm{kJ/cycle}$;
- *Hot stamping*: pump flow rate $Q_{P,CFCP} = 4545.2\,\mathrm{L\,min^{-1}}$, supply pressure $P_S = 300\,\mathrm{bar}$, corresponding hydraulic input energy $E_{in,CFCP} = 124.99\,\mathrm{MJ/cycle}$.

The constant flow rate supply pressure leads the CFCP architecture to require energy inputs $E_{in,CFCP}$ much higher than those achieved with the proposed method; due to the excess of input energy, the position control, all else being equal, is expected to be more effective. To compare the traditional to the new proposed approach, the adopted metrics therefore concern energy consumption and motion control performances. The energy saving is evaluated by calculating the percentage: $100(E_{in,CFCP} - E_{in})/E_{in,CFCP}$. The cycle times, the input energies, and the relevant energy savings for the different application cases are summarized in the first four rows of Table 1. The table shows a significant energy saving in each of the application cases. with a maximum value of 87.7%. The fifth row of Table 1 highlights for each work cycle the CO_2 emissions that can be avoided over a year thanks to the adoption of the proposed energy-saving method in plants that were previously configured according to the CFCP architecture. For this estimate, 250 yearly working days with two eight-hour shifts per day have been assumed. To convert energy into equivalent CO_2 mass, an emission factor of 0.1775 kg/kWh has been assumed; this value has been obtained from the 2025 Italian Institute for Environmental Protection and Research (ISPRA) report [50], and refers to the 2024 average value associated with the emissions involved in the total electricity production in the European Union countries.

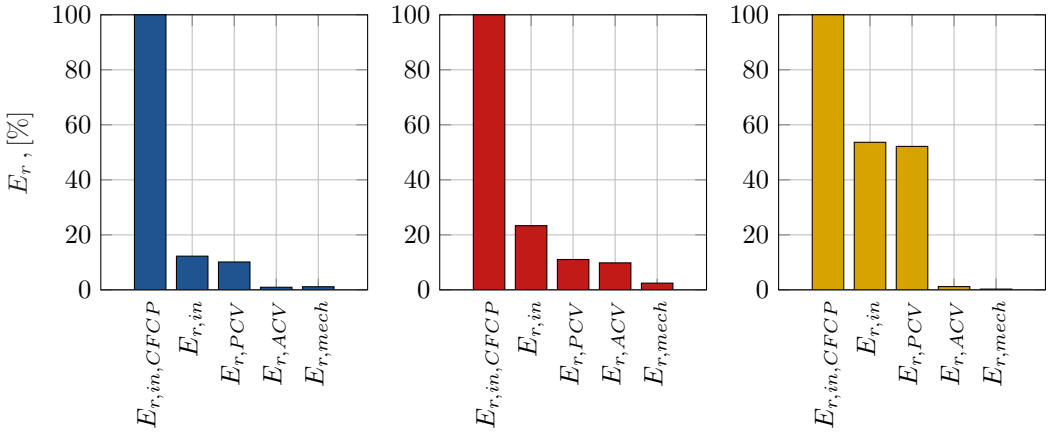
Table 1. Result summary.

	Forging	Self-Piercing Riveting	Hot Stamping
cycle time [s]	18	2.3	55
$E_{in,CFCP}$ [kJ]	10,350	18.37	124,990
E_{in} [kJ]	1268.34	4.31	67,070
Energy savings [%]	87.7	76.54	46.34
CO_2 savings [t/year]	358.2	4.3	747.7
$e_{rms,CFCP}$ [%]	0.004	0.044	0.090
e_{rms} [%]	0.283	0.203	0.169
$e_{peak,CFCP}$ [%]	0.057	0.204	0.516
e_{peak} [%]	0.583	0.803	0.769

Rows 6–9 of Table 1 report the RMS and peak errors—expressed as a percentage of the total piston displacement—achieved either with the proposed methodology or with the traditional CFCP architecture. In this respect, the CFCP configuration leads to better results, even though in all cases the RMS errors do not exceed 0.3% and the peak ones remain below 0.8%. As already remarked upon, this performance gap may be reduced in relative terms by decreasing the parameter H^*; in absolute terms, a better tuning or a refinement of the motion control system architecture could lead to improved results.

Figure 14 summarizes the energy comparison between the CFCP architecture and the proposed one. The CFCP energy consumption serves as the denominator; the first bar in

each histogram represents the reference value, $E_{r,in,CFCP} = 100E_{in,CFCP}/E_{in,CFCP}$; the second bar reports $E_{r,in} = 100E_{in}/E_{in,CFCP}$, i.e., the overall energy consumed adopting the proposed architecture; the third and fourth bars express the energy lost across the relief CCEV ($E_{r,PCV} = 100E_{PCV}/E_{in,CFCP}$) and the actuator control valve ($E_{r,SV} = 100E_{ACV}/E_{in,CFCP}$). The fifth bar reports in relative terms the energy used directly by the mechanical load, defined as $E_{r,mech} = 100(E_{in} - E_{PCV} - E_{ACV})/E_{in,CFCP}$. As already noted, relevant energy savings are achieved compared to the CFCP configuration; for the forging and hot stamping cases, the remaining energy losses occur for the greatest part across the pressure control valve; on the other hand, in the self-piercing riveting process, the losses are almost equally distributed between the two valves. This qualitative difference is due to the fact that in the riveting work cycle, the piston is almost always in motion, whereas the other two cycles display long dwell phases and slow movements.



(**a**) Forging. (**b**) Self-piercing riveting. (**c**) Hot stamping.

Figure 14. Energy consumption comparison.

5. Conclusions

This paper presented a management strategy for hydraulic actuators based on the control of the supply pressure through an innovative and unconventional use of a continuous-control electrohydraulic valve. Controlling the power supply by such means introduces substantial energy savings; moreover, the proposed technique is easily implementable on existing plants that currently rely on conventional and more energy-intensive architectures; in fact, the few required modifications have a minimal impact, mostly involving the addition of a CCEV placed downstream of the pump and towards the reservoir.

Despite this conceptual simplicity, any actual circuit modification must address additional practical issues, particularly in relation to the preexisting plant configuration. These include the comprehensive selection of valves that meet the required bandwidths and are generally suitable for the specific operating conditions, the identification of the optimal physical location for the newly installed equipment, and the effective integration of the pressure regulation loop with the already present control hardware and software.

The advantages of this solution are showcased through simulations of real case studies: forging, self-piercing riveting, and hot stamping. These three applications cover a wide range of forces; this demonstrates the validity of the proposed method for different kinds of work cycles. The simulation results, in terms of energy consumption, were compared with those obtained using the traditional Constant Flow Constant Pressure architecture; the comparison shows the significant energy saving achievable using a CCEV for supply pressure control. Significant reductions in the emission of CO_2 are consequently achieved.

The use of a continuous-control electrohydraulic valve to manage the supply pressure is, therefore, a highly effective solution for the achievement of significant energy savings in

hydraulically actuated systems. As future work, the authors are setting up a dedicated test rig to experimentally investigate the dynamic performance of the proposed architecture as a way to control the hydraulic power supply and to experimentally validate the new management and control strategy.

Author Contributions: Conceptualization, P.R. and R.S.; methodology, P.R., R.S., and F.C.; software, R.S. and F.C.; validation, P.R., R.S., F.C., J.S., and F.T.; investigation, P.R., R.S., F.C., J.S., and F.T.; writing—original draft preparation, R.S. and F.C.; supervision, P.R. All authors have read and agreed to the published version of the manuscript.

Funding: The research was funded by the University of Bergamo. Fund code: 60RIGH23.

Institutional Review Board Statement: Not applicable.

Informed Consent Statement: Not applicable.

Data Availability Statement: The original contributions presented in this study are included in the article. Further inquiries can be directed to the corresponding author.

Conflicts of Interest: The authors declare no conflicts of interest.

References

1. United Nations. Goal 9: Industry, Innovation and Infrastructure. Sustainable Development. 2015. Available online: https://sdgs.un.org/goals/goal9 (accessed on 31 March 2026).
2. Khettabi, I.; Benyoucef, L.; Boutiche, M.A. Sustainable reconfigurable manufacturing system design using adapted multi-objective evolutionary-based approaches. *Int. J. Adv. Manuf. Technol.* **2021**, *115*, 3741–3759. [CrossRef]
3. Renna, P.; Materi, S.; Ambrico, M. Review of Responsiveness and Sustainable Concepts in Cellular Manufacturing Systems. *Appl. Sci.* **2023**, *13*, 1125. [CrossRef]
4. Bataleblu, A.A.; Rauch, E.; Cochran, D.S. Model-Based Systems Engineering in Smart Manufacturing-Future Trends Toward Sustainability. In *Proceedings of the 15th International Conference on Axiomatic Design 2023*; Lecture Notes in Networks and Systems; Springer: Cham, Switzerland, 2024; Volume 849, pp. 298–311. [CrossRef]
5. Olabanji, O.M.; Mpofu, K. Design Sustainability of Reconfigurable Machines. *IEEE Access* **2020**, *8*, 215956–215976. [CrossRef]
6. He, B.; Xu, F.; Zhang, P. Kinematics approach to energy efficiency for non-holonomic underactuated robotics in sustainable manufacturing. *Int. J. Adv. Manuf. Technol.* **2022**, *119*, 1123–1138. [CrossRef]
7. Lipšinić, Z.; Husung, S.; Pavković, N.; Weber, C. Supporting circular economy strategies for design of sustainable mechatronic systems using MBSE. *Proc. Des. Soc.* **2024**, *4*, 2645–2654. [CrossRef]
8. Fedosovsky, M.E.; Uvarov, M.M.; Aleksanin, S.A.; Pyrkin, A.A.; Colombo, A.W.; Prattichizzo, D. Sustainable Hyperautomation in High-Tech Manufacturing Industries: A Case of Linear Electromechanical Actuators. *IEEE Access* **2022**, *10*, 98204–98219. [CrossRef]
9. Mai, S.T.; Ha, M.T.; Tran, T.K. Exploring synergies between industry 4.0 and circular economy for sustainable performance in manufacturing. *Discov. Sustain.* **2026**, *7*, 342. [CrossRef]
10. Martínez, M.A.D.; Rubio, Y.A.F.; Salinas, R.V.R.; Ramírez, J.R.G.; Maciel, J.D. A systematic review of Industry 5.0 and sustainability in manufacturing: Clustering of concepts, characteristics, and technological enablers. *Discov. Sustain.* **2026**, *7*, 175. [CrossRef]
11. Wang, E.; Liu, D.; Wang, S. Texture optimizing method for rotating shaft with lip seal considering processing errors. *Chin. J. Mech. Eng.* **2025**, 100199. [CrossRef]
12. Koitto, T.; Calonius, O.; Kauranne, H.; Minav, T.; Pietola, M. Enhanced energy efficiency of industrial application by direct driven hydraulic unit. In *Proceedings of the 2018 Global Fluid Power Society PhD Symposium (GFPS)*; Institute of Electrical and Electronics Engineers Inc.: New York, NY, USA, 2018; pp. 1–6. [CrossRef]
13. Yan, X.; Chen, B. Energy-efficiency improvement and processing performance optimization of forging hydraulic presses based on an energy-saving buffer system. *Appl. Sci.* **2020**, *10*, 6020. [CrossRef]
14. Yan, X.; Chen, B. Analysis of a novel energy-efficient system with a bidirectional supercharger for forging hydraulic press. *J. Clean. Prod.* **2021**, *286*, 125520. [CrossRef]
15. Liu, Y.; Shu, Y.; Xu, Z.; Zhao, X.; Chen, M. Energy efficiency improvement of heavy-load hydraulic fine blanking press for sustainable manufacturing assisted by multi-stages pressure source system. *Proc. Inst. Mech. Eng. Part B J. Eng. Manuf.* **2025**, *239*, 1166–1180. [CrossRef]

16. Li, L.; Chen, H.; Jin, R.; Xu, Y.; Liu, Q.; Li, G.; Huang, H. Independent metering-based leveling system with multi-actuator for energy saving: Modeling, control, and application on large-size forming equipment. *Energy Convers. Manag.* **2024**, *302*, 118119. [CrossRef]
17. Yan, X.; Chen, B.; Yin, F.; Ji, H.; Ma, Z.; Nie, S. Energy optimization of main hydraulic system in a forging press by simulation and experimental methods. *Energy* **2023**, *277*, 127620. [CrossRef]
18. Sumit; Gupta, D.; Juneja, S.; Nauman, A.; Hamid, Y.; Ullah, I.; Kim, T.; Tag Eldin, E.M.; Ghamry, N.A. Energy Saving Implementation in Hydraulic Press Using Industrial Internet of Things (IIoT). *Electronics* **2022**, *11*, 4061. [CrossRef]
19. Wen, C.; Li, Y.; Pan, Q.; Qu, Y.; Huang, M. Energy consumption characteristics analysis and energy-saving optimization of hydraulic forging press based on electromechanical-hydraulic coupling. *Proc. Inst. Mech. Eng. Part B J. Eng. Manuf.* **2026**. [CrossRef]
20. Yan, X.; Nie, S.; Ji, H.; Ma, Z.; Chen, B. A Novel Energy-Efficient Transmission System and Control Strategy for Hydraulic Machines. *Int. J. Energy Res.* **2023**, *2023*, 6275886. [CrossRef]
21. Ivantysynova, M. Displacement controlled linear and rotary drives for mobile machines with automatic motion control. In *International Off-Highway & Powerplant Congress & Exposition*; SAE Technical Papers; SAE International: Warrendale, PA, USA, 2000. [CrossRef]
22. Zimmerman, J.; Ivantysynova, M. Effect of Installed Hydraulic Corner Power on the Energy Consumption and Performance of Multi-Actuator Displacement Controlled Mobile Machines. In Proceedings of the ASME 2009 Dynamic Systems and Control Conference, ASME 2009 Dynamic Systems and Control Conference, Hollywood, CA, USA, 12–14 October 2009; Volume 2, pp. 871–878. [CrossRef]
23. Padovani, D.; Ivantysynova, M. Investigation of an Energy Efficient Hydraulic Propulsion System for a Railway Machine. *J. Dyn. Syst. Meas. Control* **2016**, *138*, 031009. [CrossRef]
24. Singh, S.; Kumar, A.; Thakur, S. Sustainable energy solutions for hydraulic excavators: A comprehensive review and novel energy regeneration approach. *Proc. Inst. Mech. Eng. Part E J. Process Mech. Eng.* **2025**. [CrossRef]
25. Liu, X. A review of potential energy recovery and reutilization technologies for hydraulic-driven manipulators in construction machinery. *Int. J. Mechatron. Appl. Mech.* **2025**, *1*, 59–72. [CrossRef]
26. Nguyen, V.H.; Do, T.C.; Dang, T.D.; Ahn, K.K. Improving the efficiency of hybrid hydraulic excavators with a novel powertrain and energy management system. *Energy* **2025**, *323*, 135766. [CrossRef]
27. Liang, T.; Quan, L.; Ge, L.; Xia, L.; Wang, C. An Energy-Saving Scheme to Reduce Throttling Losses in Hydraulic Excavators Based on Electro-Hydraulic Energy Storage. *IEEE Access* **2024**, *12*, 125043–125056. [CrossRef]
28. Lehto, J.; Vepsäläinen, J. Regenerative Motor Compensator for Load Sensing Hydraulics. *IEEE Access* **2026**, *14*, 41421–41430. [CrossRef]
29. Hu, B.; Fu, J.; Fan, Y.; Fu, Z. Optimal energy-saving controller design for an electro-hydrostatic actuator integrated into a wheel loader. *Adv. Mech. Eng.* **2025**, *17*. [CrossRef]
30. Zhong, Y.; Chen, W.; Chen, Z.; Zhai, G.; Ai, C.; Chen, G. Research on the global energy optimization of multi-source and multi-actuator hydraulic systems based on dynamic programming and improved adaptive genetic algorithm. *ISA Trans.* **2025**, *165*, 450–473. [CrossRef] [PubMed]
31. Stawiński, Ł.; Kosucki, A.; Skowrońska, J.; Malenta, P. Energy Efficiency Improvement of Hydraulic Indirect Elevator. *Energies* **2025**, *18*, 2163. [CrossRef]
32. Dong, J.; Jin, B.; Liu, Z.; Chen, L. Energy-Efficient Hydraulic System for Hexapod Robot Based on Two-Level Pressure System for Oil Supply. *Biomimetics* **2025**, *10*, 151. [CrossRef]
33. Li, L.; Cheng, M.; Ding, R.; Xu, B. Energy Efficiency Improvement of Hydraulic Manipulator Through Flow-Optimal Redundancy Resolution With Path Following. *IEEE Trans. Autom. Sci. Eng.* **2025**, *22*, 7870–7886. [CrossRef]
34. Rustamov, K.J.; Rustamova, N.R. Advanced hydraulic drive systems in multi-purpose machinery: Enhancing efficiency and performance in modern engineering. *AIP Conf. Proc.* **2025**, *3304*, 030093. [CrossRef]
35. Ho, T.H.; Le, T.D. Development and Evaluation of Energy-Saving Electro-Hydraulic Actuator. *Actuators* **2021**, *10*, 302. [CrossRef]
36. Righettini, P.; Strada, R.; Tiboni, M.; Cortinovis, F.; Santinelli, J. A systematic management and control methodology for high energy saving in applications equipped with hydraulic servo-axes. *Control Eng. Pract.* **2024**, *145*, 105847. [CrossRef]
37. Righettini, P.; Strada, R.; Cortinovis, F. Load Simulator Design for the Experimental Validation of a High Energy Saving Methodology in the Automation System of Hydraulic Presses. In Proceedings of the 2024 International Congress on Human-Computer Interaction, Optimization and Robotic Applications (HORA), Istanbul, Turkiye, 23–25 May 2024; pp. 1–9. [CrossRef]
38. Guglielmino, E.; Edge, K.A. Modelling of an Electrohydraulically-Activated Friction Damper in a Vehicle Application. In *ASME International Mechanical Engineering Congress and Exposition*; Volume Fluid Power Systems and Technology; American Society of Mechanical Engineers: New York, NY, USA, 2001; pp. 153–161. [CrossRef]
39. Guglielmino, E.; Edge, K.A. A controlled friction damper for vehicle applications. *Control Eng. Pract.* **2004**, *12*, 431–443. [CrossRef]

40. Righettini, P.; Strada, R.; Cortinovis, F.; Santinelli, J. New Management Strategy for a Significant Reduction of the Impact on CO2 Footprint of Hydraulic Actuators. *Mech. Mach. Sci.* **2025**, *179*, 505–512. [CrossRef]
41. Akers, A.; Gassman, M.; Smith, R. *Hydraulic Power System Analysis*; CRC Press: Boca Raton, FL, USA, 2006. [CrossRef]
42. Rydberg, K.E. *Hydraulic Servo Systems: Dynamic Properties and Control*; Linkoping University Electronic Press: Linkoping, Sweden, 2016. Available online: https://nbn-resolving.org/urn:nbn:se:liu:diva-132396 (accessed on 9 January 2026).
43. Righettini, P.; Strada, R.; Valilou, S.; Khademolama, E. Nonlinear Modeling and Experimental Validation of Uni-Axial Servo-Hydraulic Shaking Table. In *Proceedings of the BATH/ASME 2016 Symposium on Fluid Power and Motion Control, Fluid Power Systems Technology*; American Society of Mechanical Engineers: New York, NY, USA, 2016; p. V001T01A037. [CrossRef]
44. Righettini, P.; Strada, R.; Valilou, S.; Khademolama, E. Gray-box acceleration modeling of an electro hydraulic servo shaking table with neural network. In Proceedings of the IEEE/ASME International Conference on Advanced Intelligent Mechatronics, Munich, Germany, 3–7 July 2017; pp. 1388–1392. [CrossRef]
45. Zhao, K.; Liu, Z.; Yu, S.; Li, X.; Huang, H.; Li, B. Analytical energy dissipation in large and medium-sized hydraulic press. *J. Clean. Prod.* **2015**, *103*, 908–915. [CrossRef]
46. Li, L.; Huang, H.; Zhao, F.; Liu, Z. Operation scheduling of multi-hydraulic press system for energy consumption reduction. *J. Clean. Prod.* **2017**, *165*, 1407–1419. [CrossRef]
47. Haque, R.; Durandet, Y. Investigation of self-pierce riveting (SPR) process data and specific joining events. *J. Manuf. Process.* **2017**, *30*, 148–160. [CrossRef]
48. Tang, D.; Evans, M.; Briskham, P.; Susmel, L.; Sims, N. Dynamic Modelling of a Servo Self-Pierce Riveting (SPR) Process. *Proc. Inst. Mech. Eng. Part B J. Eng. Manuf.* **2021**, *235*, 2052–2065. [CrossRef]
49. Zhang, Y.; Wang, L.; Wang, Y.; Zhu, B.; Su, Z.; Du, Y.; Zhang, W.; Chai, X.; Deng, S.; Ren, X. Research on Hot Stamping Production Line and Digital Twin System Based on Industry 4.0. In *Proceedings of the 7th International Conference on Advanced High Strength Steel and Press Hardening (ICHSU 2024)*; Atlantis Highlights in Materials Science and Technology; Atlantis Press: Dordrecht, The Netherlands, 2024; Volume 3, pp. 471–486. [CrossRef]
50. Caputo, A. *Efficiency and Decarbonization Indicators in Italy and in the Biggest European Countries*; Technical Report 418/25; Italian Institute for Environmental Protection and Research: Roma, Italy, 2025.

Disclaimer/Publisher's Note: The statements, opinions and data contained in all publications are solely those of the individual author(s) and contributor(s) and not of MDPI and/or the editor(s). MDPI and/or the editor(s) disclaim responsibility for any injury to people or property resulting from any ideas, methods, instructions or products referred to in the content.